Origins of the Ultrashort-T_2 ^{1}H NMR Signals in Myelinated Nerve: A Direct Measure of Myelin Content?

R. Adam Horch[1,2], **John C. Gore**[1,2,3,4], and **Mark D. Does**[1,2,3,5]

[1]Dept. of Biomedical Engineering, Vanderbilt University

[2]Institute of Imaging Science, Vanderbilt University

[3]Radiology and Radiological Sciences, Vanderbilt University

[4]Molecular Physiology and Biophysics, Vanderbilt University

[5]Electrical Engineering, Vanderbilt University

Abstract

Recently developed MRI techniques have enabled clinical imaging of short-lived ^{1}H NMR signals with $T_2 < 1$ ms. Using these techniques, novel signal enhancement has been observed in myelinated tissues, although the source of this enhancement has not been identified. Herein, we report studies of the nature and origins of ultra-short T_2 (uT_2) signals (50 μs $< T_2 < 1$ ms) from amphibian and mammalian myelinated nerves. NMR measurements and comparisons with myelin phantoms and expected myelin components indicate that these uT_2 signals arise predominantly from methylene ^{1}H on/in the myelin membranes, which suggests that direct measurement of uT_2 signals can be used as a new means for quantitative myelin mapping.

Keywords

MRI; myelin; T_2; ultra short TE; magnetization transfer

Introduction

Quantitative myelin imaging is of widespread interest for both clinical and research studies of a number of neurological disorders, including Multiple Sclerosis, Alzheimer's Disease, various leukodystrophies, and numerous psychiatric disorders. For almost two decades the MRI research community has pursued the development and experimental validation of quantitative myelin mapping, primarily through one of three approaches: diffusion tensor imaging (DTI), quantitative magnetization transfer (qMT), and multi-exponential T_2 (MET$_2$). In lieu of a detailed discussion of these efforts, we direct the reader to a comprehensive review article by Laule and colleagues (1). Briefly though, while DTI has great sensitivity to white matter microstructure, it has not been found to be specific to myelin. Both qMT and MET$_2$ have shown greater promise to be more specific, but neither has been widely adopted because of the remaining ambiguity in interpretation and difficulty of fast, multi-slice or 3D implementation. Another approach, which has thus far garnered relatively little attention, is the imaging of ultra-short T_2 (< 1 ms) signals using ultra-short Echo Time (uTE) imaging (2), or related methods (3,4). uTE methods have demonstrated relatively greater signal in white matter compared to gray (5,6), but no studies (to our

knowledge) have yet evaluated the origins of this signal or its relationship to myelin. Presented here are ^{1}H NMR measurements and isotopic perturbations on both central and peripheral nerves as well as on myelin phantoms, which were used to characterize and determine the biophysical origins of ultra-short T_2 (uT_2) signals (50 μs < T_2 < 1 ms) in myelinated tissue. Results indicate that uTE MRI has promise as a specific measure of myelin content.

Methods

NMR

^{1}H NMR measurements were performed at 200 MHz in a 31-cm horizontal bore 4.7T magnet, equipped with a Varian DirectDrive Console (Varian Medical Systems, Palo Alto, CA). An in-house built 10-mm diameter loop-gap RF coil with Teflon structural support and low background ^{1}H signal (similar to the lowest-proton design described in (7)), was used for all measurements.

The Carr-Purcell-Meiboom-Gill (CPMG) (8) pulse sequence was used to measure transverse relaxation in each sample with the following experimental parameters (based on a previous study of cortical bone (9)): 10000 echoes, 100 μs echo spacing (first echo at 100 μs), ≈ 6.5/13 μs (90°/180°) RF pulse durations, 40 μs signal acquisition time per echo, 15 s TR, 16 averaged excitations and a four-part $90_{(x,-x,x,-x)}$/$180_{(y,y,-y,-y)}$ phase cycling scheme. Free induction decays (FIDs) were also collected using ≈ 6.5 μs-duration 90°-pulse, 2.5 MHz bandwidth acquisition, 15 s TR, and 64 averaged excitations with a $90_{(x,y,-x,-y)}$ phase cycling scheme. After receiver dead time and coil ringing, the first FID sample was acquired 10.4 μs after the midpoint of the 90°-pulse.

From each CPMG acquisition, a T_2 spectrum was estimated by forming a linear system equating the signal (10,000 echoes) to a sum of 128 exponential functions (time constants log-spaced between 10 μs and 1 sec), reducing the system dimension by singular value decomposition (10), then fitting exponential amplitudes in a non-negative least-squares sense and subject to a minimum curvature regularization (10,11). The regularization was adjusted to a conservative level by matching T_2 spectral features in the 10-300 ms range to those in previous studies (12,13). T_2^* spectra were estimated similarly from the first ≈500 μs of the FIDs and with time constants between 5 and 2000 μs. Because previous studies of a model membrane system similar to myelin have demonstrated non-exponential free induction decays (FIDs) (14,15), (which would appear similarly in a CPMG measurement), non-exponential decay characteristics were also investigated in the deuterated myelin extract and phantom measurements. Fitted CPMG and FID components with T_2 (or T_2^*) > 200 μs were subtracted from the original signals to isolate the shortest-lived signal components, which were then fitted to a Gaussian function by nonlinear regression.

T_2-T_2 relaxation exchange spectroscopy (REXSY) (16,17) was used to identify magnetization exchange between T_2 components, and was implemented with the following experimental parameters: 15 s TR, 53 different CPMG preparation times pseudo log-spaced between 100 μs and 1 s, a 200 ms mixing time, and a CPMG acquisition as described above (10000 echoes at 100 μs echo spacing, etc). Four excitations were collected with a 2-step phase cycle of the storage pulse, resulting in a total scan time of ≈ 60 min. REXSY echo magnitudes were reduced by singular-value decomposition prior to two-dimensional non-negative least squares fitting (18,19) to the aforementioned range of decaying exponentials, producing a so-called T_2-T_2 spectrum.

All measurements were made at bore temperature (≈ 20°C) and all data processing (REXSY and CPMG) was performed using MATLAB (The Mathworks, Natick, MA) and the freely-

available MERA_Toolbox (Multi-Exponential Relaxation Analysis, http://vuiis.vanderbilt.edu/~doesmd/MERA/MERA_Toolbox.html).

Nerve

Immediately following euthanasia, a pair of sciatic nerves were excised from each of three frogs (adult African clawed toads—Xenopus laevis) to characterize peripheral nerve, and a pair of optic nerves were excised from each of two rats (adult Sprague-Dawley) to characterize nerve more similar to the central nervous system. All animal handling protocols were approved by the Vanderbilt University Institutional Animal Care and Use Committee.

From each frog, $\approx$ 20 mm of sciatic nerve was extracted from each hind limb using blunt dissection techniques. Samples were cleaned of blood and connective tissue and stored in buffered isotonic solutions. One nerve sample was placed in amphibian Ringer's solution (Fisher Scientific, Waltham, MA) and the other in a mixture of D_2O (99.9% isotopic purity, Sigma-Aldrich Corp., St. Louis, MO) and electrolytes (by mass proportion: 73 NaCl : 2 KCl : 1 $CaCl_2$: 2 $NaHCO_3$) consistent with amphibian Ringer's solution. From each rat, $\approx$ 5 mm from each optic nerve was extracted from a span between the skull and optic chiasm, cleaned of blood and connective tissue and stored in buffered isotonic solutions. One nerve sample was placed in a standard phosphate buffered saline (PBS) solution (Mediatech Inc., Manassas, VA) and the other in a deuterated solution made by mixing D_2O (above) with the appropriate mass PBS electrolyte tablets (MP Biomedicals, Solon, OH).

Both sciatic and optic nerve samples were maintained on a shaker table at 4 °C and agitated at 20 RPM. Periodically, over a three-hour duration, samples were removed from the buffer and placed in a 5-mm o.d. NMR tube filled with Fomblin (a ^1H-free oil, Solvay Solexis, West Deptford, NJ) for CPMG measurements ($\approx$ 5 min). Following data collection, the samples were returned to the appropriate buffer. After three hours, the sciatic nerve samples that were stored in regular Ringer's solution were again placed in a 5-mm o.d. NMR tube filled with Fomblin for REXSY measurements ($\approx$ 60 min).

Tissue Phantoms

In addition to the study of freshly excised nerve, three tissue phantoms were studied: I) a biologically-derived myelin extract phantom, II) a synthetic myelin lipid phantom, and IIIa/b) two protein phantoms. All tissue phantoms were prepared in both hydrated and deuterated states and studied with CPMG, as described above.

Phantom I, biologically-derived myelin extract, was formulated from bovine brain myelin extract as follows: Folch Fraction I (Type-I bovine brain extract, Sigma-Aldrich Corp., St. Louis, MO), an organophilic extract of predominantly myelin-related brain lipids (20), was lightly milled with mortar and pestle into a fine powder and lyophilized at 0.05 mBar for 24 hours to remove water and residual solvents. The remaining powder (50 mg) was then combined via high-speed vortexer with 35 μL of either deionized water or D_2O, forming paste-like phantoms with the solid-liquid mass ratio = 3:2, as expected in physiological myelin.

Phantom II, synthetic myelin lipid, was formulated to approximate the non-protein portion of biological myelin, and consisted of 50% (w/w) deionized water (or D_2O), 13.5% cholesterol, 13% galactocerebroside, 19.3% phosphatidylcholine, and 4.2% sphingomyelin (all lipids obtained from Sigma-Aldrich Corp., St. Louis, MO). The solid lipid mixture (50 mg) was co-solvated in 150 μL of a 2:1 (by volume) mixture of chloroform:methanol to uniformly incorporate all components. The resulting solution was then lyophilized for 48 hours to remove all solvents and residual water, and the recovered residue was combined with the appropriate amount of either water or D_2O via high-speed vortexer.

Two aqueous protein phantoms were prepared: Phantom IIIa consisted of 20% w/w Type-1 collagen, purified from bovine tendon (Sigma-Aldrich Corp., St. Louis, MO), and Phantom IIIb consisted of a gel of 20% w/w bovine serum albumin (99.9% purity, Sigma-Aldrich Corp., St. Louis, MO), crosslinked with 25 μL/mL of 50% aqueous glutaraldehyde (Electron Microscopy Sciences, Hatfield, PA).

Results

Typical T_2 spectra from nerve samples ≈1.5 hr in control and deuterated buffer, and from tissue phantoms, in hydrated and deuterated states, are shown in Fig 1. Note that although the vertical scales in Fig 1 are in arbitrary units, we know from previous experience with this experimental set-up that the inter-sample variation in ^{1}H NMR signal amplitude between like samples is ≈ 5% (9), so it is reasonable to compare spectra from control and deuterated samples on the same scale. Control nerve T_2 spectra are generally similar to previously published results for frog sciatic (12) and rat optic (13) nerve, with a few exceptions. Most importantly, previous studies did not investigate the sub-millisecond T_2 domain where Fig 1 shows two signal components in both frog sciatic ($T_2 \approx 50$ μs and ≈ 250 μs) and rat optic nerve ($T_2 \approx 80$ μs and ≈ 700 μs) spectra. As also seen in Fig 1, these uT_2 signals did not wash out during immersion of nerves in deuterated buffer, despite the loss of ≈95% of frog sciatic nerve long-T_2s (>1 ms, as consistent with a previous study (21)) and ≈68% of rat optic nerve long-T_2s. Repeat CPMG measures during immersion confirmed that a steady-state condition was reached in frog sciatic nerve within the first 1.5 hr of D_2O immersion. The long-T_2s in the rat optic nerve did not reach a clear steady-state within two hours of immersion, at which point the nerve had begun to visibly disintegrate, so one additional rat optic nerve was fixed in glutaraldehyde/formalin and followed over a 10-day period of D_2O immersion. These data (not shown) indicated that 82% of the initial long-T_2s were removed by D_2O immersion, while uT_2s remained unchanged. The remaining long T_2 signal from deuterated rat optic nerve was on the same order of magnitude as the known background signal from the coil and ambient water vapor (7), which is negligible compared to the much larger signals from the sciatic nerves and phantoms.

The resilience of the uT_2 signals in nerve to the deuterated buffers indicate that they are *not* derived from water protons or chemically-exchangeable amide/hydroxyl protons, but rather must predominantly arise from carbon-bound methylene protons. Similar uT_2 signal components which are also present in both hydrated and deuterated states, are seen in Phantom I (myelin extract) and Phantom II (myelin lipids), which suggests that myelin and/ or other membrane lipids may be the source of these methylene protons which give rise to the uT_2 signals. Conversely, the absence of uT_2 components from Phantom III (protein solutions) suggests that tissue proteins are not a likely source. (Due to the absence of uT_2 signals, Phantom III preparations were not further studied in a deuterated state.)

Figure 2 shows the T_2-T_2 spectra from REXSY measurements of a frog sciatic nerve (representative of both frogs studied). Although this T_2-T_2 spectrum is unregularized, it is readily apparent that the main diagonal is similar to the CPMG-derived T_2 spectrum from frog nerve in Fig 1. The off-diagonal components indicate exchange of magnetization between corresponding main-diagonal T_2 components during the 200 ms mixing period. As such, Fig 2 indicates exchange between the dominant uT_2 component and both the 25 ms and 90 ms T_2 components. Possible exchange between the 20 ms and the 90 ms T_2 components is indicated by the presence of one cross peak, while the 300 ms component apparently does not exchange with any components on the timescale of the 200 ms mixing period. REXSY measurement of the myelin extract phantom (Fig 2) also indicates magnetization exchange between its uT_2 and ≈ 15 ms T_2 water component.

Figure 3A-C shows FID and CPMG signals (3A) and corresponding multi-exponential fits (3B) from the deuterated myelin extract (Phantom I). When stripped of long-lived components (T_2 or $T_2^* > 200$ μs), the signals fitted to both exponential and Gaussian functions are shown in Fig 3C. These fits indicate that if the short-lived CPMG signal decayed according to a Gaussian function, then the exponential fitting used here could overestimate this component amplitude by as much as ≈2.5×. However, the FID did not reveal such a prominent Gaussian decay characteristic and restricted this overestimation to ≈10%. The residual second moments from Gaussian fits did not exceed 1.1×10^9 s^{-2} across all nerves and myelin phantoms, which is consistent with a dipolar-broadened liquid crystalline lipid system (15). Such a system is theoretically described by a super-Lorentzian lineshape, as previously experimentally shown for non-aqueous signals from whole cells (14). The super-Lorentzian deviates from an exponential shape to a lesser extent than the Gaussian, so while it is generally inaccurate to model a dipolar-broadened spin system with exponential basis functions, the inaccuracy in fitted signal amplitudes is small in this case. To be clear, we are not arguing that a dipolar-broadened non-aqueous tissue signal is theoretically described by Lorentzian lineshape. In Fig 3D&E, FID data and exponential fits are shown for a representative sciatic nerve and phantoms, and it is clear that the sciatic nerve possesses a uT_2 component (≈ 70 μs) similar to the myelin phantoms, as well as shorter-lived component (< 20 μs) similar to the two protein phantoms.

Discussion

In amphibian and mammalian myelinated nerves, previous studies have thoroughly characterized T_2 components with relaxation times greater than 1 ms, and our observations over this T_2 domain are in good agreement with these studies (12,13). In these, the $T_2 \approx 20$ ms component has been attributed to myelin water; consequently, in this study, signals with 1 ms < T_2 < 50 ms are defined as arising from myelin water. In contrast, uT_2 signals (50 μs < T_2 < 1 ms) from myelinated tissues have not been well studied. Previous uTE imaging studies have demonstrated greater signal in white matter compared to grey matter (5,6), and numerous magnetization transfer (MT) studies have modeled white matter as having a greater reservoir of solid/semi-solid protons (typically modeled with $T_2 \approx 10$ μs) compared to grey matter (22-25), but, to our knowledge, no previous study has directly measured a range of sub-millisecond T_2 components and attempted to determine their biophysical origins. (Again, describing these signal components with T_2 time constants is done for convenience and not to imply that they are truly governed by exponential decay functions.)

The finding that uT_2 components survive D_2O immersion in all nerves (Fig 1) but still exchange magnetization with known water components on a 200 ms time scale (Fig 2) indicates that uT_2 signals cannot predominantly arise from water or water-exchangeable ^{1}H, including those found on mobile and bound water in the intra/extra-axonal or myelin spaces. If the uT_2 components were to arise from water, it is not conceivable how they could both survive D_2O immersion and directly exchange with water that is lost to D_2O immersion. Rather, we suggest that the nerve uT_2 signal primarily arises from the methylene ^{1}H, for which there are two broad sources: phospholipid membranes and various intra- and extra-cellular proteins.

The biological myelin extract phantom (I) exhibited a similar methylene uT_2 ^{1}H signal to that found in the myelinated nerves (Figs 1&3). This observation demonstrates that myelin is a source for the uT_2 signal, but does not itself discriminate lipid from protein sources, nor does it define the relative contribution of myelin to the uT_2 signal. Although known to be predominantly lipids, the exact chemical composition of Phantom I was not determined and thus it cannot be used to rule out a protein source. However, in comparing the observations from Phantoms II and III, we see that both hydrated and deuterated lipids known to exist in

myelin membrane exhibited uT_2 signals, while no such signal in the 50-1000 μs domain was found from either the Type-I collagen or BSA phantoms (Fig 3D&E). Of course, there are many proteins in tissue, but collagen is representative of a large fraction of extra-cellular matrix proteins in nerve, and BSA is a common model for intra-axonal and membrane proteins. It is possible that methylene protons in nerve proteins contribute to an even shorter-lived ≈10 μs T_2 component, which has been previously characterized through MT measurements (22,23,25) and through wideline FIDs (24). As shown in Fig 3, such a component was observed in the FIDs acquired from nerves and protein phantoms (III a/b) but not from the myelin extract (I) or lipid phantoms (II). Additionally, the deuterated forms of phantoms I and II were prepared from anhydrous starting materials, so their sizeable uT_2 signals cannot originate from a trapped water compartment that is D_2O-inaccessible. Combining this with the noted uT_2 similarities between nerves and phantoms I/II further suggests that the nerve uT_2s do not arise from water. With these findings, we conclude that the uT_2 signal from nerve is predominately derived from membrane lipids.

To evaluate the relative contribution of myelin to the uT_2 signal, consider the relative sizes of the uT_2 and myelin water signals. In both sciatic and optic nerve, the methylene uT_2 signal is approximately equal to the size of the myelin water signal (Fig 1 and Table 1). While there is no known source of lipid outside the myelin that alone can account for such a significant tissue volume, it is possible that some uT_2 signal is derived from non-myelin lipid sources. These sources include plasma and organelle membranes, which represent a minor fraction of the total lipid content in myelinated nerve, so we expect the observed uT_2 signals in myelinated nerves to be strongly myelin-specific.

Additionally, because the chemical composition of myelin has been well studied, the postulate of a uT_2 myelin methylene proton origin can be evaluated by comparing the relative sizes of observed uT_2 and myelin water signals to the expected relative amounts of myelin membrane-associated ^1H and myelin water. To this end, the ^1H content of model myelin can be estimated from established compositional information. Assume i) that myelin contains 40% water and 60% solids (by mass) (1,26); ii) that the solid portion of myelin contains 20% protein and 80% lipids (by mass) (1,26); iii) the composition of the protein portion to be a 3:5 mixture (by mass) (1) of myelin basic protein ($C_{471.3}H_{834.8}N_{152}O_{142.7}S_{1.2}$ with 304.5 non-methylene ^1H) and proteolipid protein ($C_{486.5}H_{846.1}N_{115.8}O_{138.9}S_{5.9}$ with 256.7 non-methylene ^1H), respectively (non-stoichiometric empirical formulas are derived from bovine myelin shown in (27)); and, iv) from (26), the composition of the lipid portion to be: 27% cholesterol ($C_{27}H_{46}O$ with one non-methylene ^1H), 26% gangliosides (assume GM1: $C_{73}H_{131}N_3O_{31}$ with 20 non-methylene ^1H), 20% phosphatidylethanolamine ($C_{37}H_{75}NO_8P$ with four non-methylene ^1H), 10% phosphatidylcholine ($C_{40}H_{81}NO_8P$ with one non-methylene ^1H), 8.5% phosphatidylserine ($C_{38}H_{74}NO_{10}P$ with four non-methylene ^1H), and 8.5% sphingomyelin ($C_{38}H_{78}N_2O_6P$ with three non-methylene ^1H); palmitate fatty acids were assumed for the phosphatidyl- and sphingomyelin structures.

Then, from this model myelin composition, the relative proportions of each myelin component's expected ^1H pool size were derived and are shown in Fig 4. From these proportions, it is straightforward to calculate the expected ratio of myelin methylene ^1H to myelin water (≈1.21, Table 1), which is similar to the observed values of ≈1.11 (bovine myelin extract), ≈1.12 (rat optic nerve) and ≈0.98 (frog sciatic nerve). Further, if we consider only the lipid contribution, as argued by observations from Phantoms I-III, this expected ratio drops from 1.21 to 1.07, which is even closer to the observed ratios and further suggests that proteins do not significantly contribute to the uT_2 signals. Hence, the assertion that the uT_2 signal from nerve is predominantly due to myelin is consistent with the comparison of the uT_2 signal amplitude and the known composition of myelin. And,

while the reported uT_2 signal sizes are subject to experimental error and possible modest overestimation due to non-exponential decay characteristics (see Fig 3), there are clearly *enough* methylene ^1H in myelin membranes to account for the observed uT_2 signal sizes.

Results from REXSY measurements offer further insight into the nature of the uT_2 signals components in nerve. REXSY spectra (Fig 2) from both sciatic nerve and myelin extract demonstrate exchange of magnetization between the uT_2 signal and the myelin water signal (as well as some longer-lived T_2 components in nerve). This exchange must be mediated at some point by a through-space dipolar interaction, since the methylene ^1H responsible for uT_2 signals will not chemically exchange with water ^1H. Previous work has demonstrated such an interaction between methylene ^1H and water (28). However, other studies have presented compelling evidence that commonly observed MT in myelinated tissue is mediated by chemical exchange of water protons with head-group $-OH$ protons on cholesterol (29) and, more significantly, on membrane lipids such as galactocerebroside (30). We postulate that the relatively large membrane lipid methylene ^1H pool, responsible for the uT_2 signal, acts as a spin reservoir that supplies the less abundant surface $-OH$ proton pool with magnetization via spin diffusion from the membrane interior to the water-accessible surface groups. The extent to which this magnetization exchange pathway contributes the commonly observed MT contrast in white matter is not clear, but the REXSY observations indicate that a two-pool MT model containing a $T_2 \approx 10$ µs solid ^1H pool as the only submillisecond-T_2 species is probably incomplete for characterizing MT in myelinated tissue.

In comparison to other myelin imaging methods, quantitative imaging of the uT_2 signal is potentially more myelin-specific and easier to measure. As noted above, the uT_2 signal likely contributes to qMT measures of the solid pool size (M_{0b}), but it is additional to and distinct from the $T_2 \approx 10$ µs signal, which was observed in FIDs from whole nerve but not myelin extract. This suggests that the uT_2 signal is derived from a sub-set—possibly more myelin-specific—of spins that contribute to M_{0b}, and simple two-compartment modeling (semisolid & liquid spin pools) may be inadequate. Also, current qMT methods require several acquisitions and non-linear signal modeling, e.g., (25,31), but the similarity between T_2 and T_2^* spectra from myelin extract (Fig 3b) indicates that the uT_2 signal ($T_2 \approx 50\text{-}150$ µs) is accessible to standard uTE methods with minimal signal processing. In comparison to myelin water fraction (MWF) derived from multi-exponential analysis of water signal (32), it is much easier in principle to distinguish a uT_2 signal from tissue water signals ($T_2s = 10\text{-}100$ ms) than it is to distinguish "myelin water" ($T_2 \approx 20$ ms) from non-myelin water ($T_2 \approx 80$ ms). Also, the much shorter T_2 of the uT_2 signal makes its amplitude less sensitive to magnetization exchange with other spin pools. Inter-compartmental water exchange, as affected by myelin thickness, appears to contribute to the MWF in rat spinal white matter (33), although the effect in brain remains unknown. Ultimately, the relationship between the uT_2 signal and other MRI measures of myelin, and to myelin content and structure itself, will require further studies.

Conclusions

In summary, methylene ^1H NMR signals with $T_2 = 50$ µs to 1 ms and similar in amplitude to the myelin water signal ($T_2 = 10\text{-}50$ ms) are reported in both amphibian and mammalian myelinated nerves. Combined evidence from ^1H isotopic manipulation, relaxation-based exchange spectroscopy, and measurements of multiple tissue phantoms indicates that these signals predominantly originate from methylene ^1H on/in the myelin membranes. As such, the uT_2 signals likely provide a direct measure of myelin content that is more accessible than the myelin water signal because of T_2 isolation. We expect the uT_2 signals reported herein to

be present in all myelinated tissues, and it is likely that such signals are the source of previously reported white matter contrast enhancement in uTE images.

Acknowledgments

References

1. Laule C, Vavasour IM, Kolind SH, Li DKB, Traboulsee TL, Moore GRW, MacKay AL. Magnetic resonance imaging of myelin. Neurotherapeutics. 2007; 4(3):460–484. [PubMed: 17599712]

2. Robson MD, Gatehouse PD, Bydder M, Bydder GM. Magnetic resonance: An introduction to ultrashort TE (UTE) imaging. J Comput Assist Tomogr. 2003; 27(6):825–846. [PubMed: 14600447]

3. Wu YT, Ackerman JL, Chesler DA, Graham L, Wang Y, Glimcher MJ. Density of organic matrix of native mineralized bone measured by water- and fat-suppressed proton projection MRI. Magn Reson Med. 2003; 50(1):59–68. [PubMed: 12815679]

4. Idiyatullin D, Corum C, Park JY, Garwood M. Fast and quiet MRI using a swept radiofrequency. Journal of Magnetic Resonance. 2006; 181(2):342–349. [PubMed: 16782371]

5. Gatehouse PD, Bydder GM. Magnetic resonance imaging of short T-2 components in tissue. Clinical Radiology. 2003; 58(1):1–19. [PubMed: 12565203]

6. Waldman A, Rees JH, Brock CS, Robson MD, Gatehouse PD, Bydder GM. MRI of the brain with ultra-short echo-time pulse sequences. Neuroradiology. 2003; 45(12):887–892. [PubMed: 14508620]

7. Horch RA, Wilkens K, Gochberg DF, Does MD. RF Coil Considerations for Short-T_2 MRI. Magn Reson Med. 2010; 64(6):1652–1657. [PubMed: 20665825]

8. Meiboom S, Gill D. Modified Spin-Echo Method for Measuring Nuclear Relaxation Times. Review of Scientific Instruments. 1958; 29(8):688–691.

9. Horch RA, Nyman JS, Gochberg DF, Dortch RD, Does MD. Characterization of 1H NMR Signal in Human Cortical Bone for Magnetic Resonance Imaging. Magn Reson Med. 2010; 64(3):680–687. [PubMed: 20806375]

10. Lawson, CL.; Hanson, RJ. Solving least squares problems. Philadelphia: SIAM; 1995. p. xiip. 337

11. Whittall KP, Mackay AL. Quantitative interpretation of NMR relaxation data. Journal of Magnetic Resonance. 1989; 84(1):134–152.

12. Does MD, Beaulieu C, Allen PS, Snyder RE. Multi-component T-1 relaxation and magnetisation transfer in peripheral nerve. Magn Reson Imaging. 1998; 16(9):1033–1041. [PubMed: 9839987]

13. Bonilla I, Snyder RE. Transverse relaxation in rat optic nerve. Nmr Biomed. 2007; 20(2):113–120. [PubMed: 16998953]

14. Bloom M, Holmes KT, Mountford CE, Williams PG. Complete Proton Magnetic Resonance in Whole Cells. Journal of Magnetic Resonance. 1986; 69(1):73–91.

15. MacKay AL. A proton NMR moment study of the gel and liquid-crystalline phases of dipalmitoyl phosphatidylcholine. Biophys J. 1981; 35(2):301–313. [PubMed: 6895041]

16. Lee JH, Labadie C, Springer CS, Harbison GS. Two-dimensional inverse laplace transform NMR: altered relaxation times allow detection of exchange correlation. J Am Chem Soc. 1993; 115:7761–7764.

17. Callaghan PT, Arns CH, Galvosas P, Hunter MW, Qiao Y, Washburn KE. Recent Fourier and Laplace perspectives for multidimensional NMR in porous media. Magn Reson Imaging. 2007; 25(4):441–444. [PubMed: 17466759]

18. English AE, Whittall KP, Joy MLG, Henkelman RM. Quantitative 2-dimensional time correlation relaxometry. Magn Reson Med. 1991; 22(2):425–434. [PubMed: 1812377]

19. Venkataramanan L, Song YQ, Hurlimann MD. Solving Fredholm integrals of the first kind with tensor product structure in 2 and 2.5 dimensions. Ieee Transactions on Signal Processing. 2002; 50(5):1017–1026.

20. Folch J. Brain cephalin, a mixture of phosphatides. Separation from it of phosphatidyl serine, phosphatidyl ethanolamine, and a fraction containing an inositol phosphatide. Journal of Biological Chemistry. 1942; 146(1):35–44.

21. Wachowicz K, Snyder RE. Assignment of the T-2 components of amphibian peripheral nerve to their microanatomical compartments. Magn Reson Med. 2002; 47(2):239–245. [PubMed: 11810666]

22. Morrison C, Henkelman RM. A Model for Magnetization-Transfer in Tissues. Magn Reson Med. 1995; 33(4):475–482. [PubMed: 7776877]

23. Stanisz GJ, Kecojevic A, Bronskill MJ, Henkelman RM. Characterizing white matter with magnetization transfer and T-2. Magn Reson Med. 1999; 42(6):1128–1136. [PubMed: 10571935]

24. Bjarnason TA, Vavasour IM, Chia CLL, MacKay AL. Characterization of the NMR behavior of white matter in bovine brain. Magn Reson Med. 2005; 54(5):1072–1081. [PubMed: 16200557]

25. Gochberg DF, Gore JC. Quantitative magnetization transfer imaging via selective inversion recovery with short repetition times. Magn Reson Med. 2007; 57(2):437–441. [PubMed: 17260381]

26. Gennis, RB. Biomembranes : molecular structure and function. New York: Springer-Verlag; 1989. p. xviip. 23

27. Greenfield S, Brostoff S, Eylar EH, Morell P. Protein composition of myelin of the peripheral nervous system. Journal of Neurochemistry. 1973; 20(4):1207–1216. [PubMed: 4697881]

28. Gore JC, Brown MS, Armitage IM. An analysis of magnetic cross-relaxation between water and methylene protons in a model system. Magn Reson Med. 1989; 9(3):333–342. [PubMed: 2540400]

29. Koenig SH. Cholesterol of myelin is the determinant of gray-white contrast in MRI of brain. Magn Reson Med. 1991; 20(2):285–291. [PubMed: 1775053]

30. Kucharczyk W, Macdonald PM, Stanisz GJ, Henkelman RM. Relaxivity and magnetization transfer of white matter lipids at MR imaging: importance of cerebrosides and pH. Radiology. 1994; 192(2):521–529. [PubMed: 8029426]

31. Sled JG, Pike GB. Quantitative imaging of magnetization transfer exchange and relaxation properties in vivo using MRI. Magn Reson Med. 2001; 46(5):923–931. [PubMed: 11675644]

32. Mackay A, Whittall K, Adler J, Li D, Paty D, Graeb D. In vivo visualization of myelin water in brain by magnetic resonance. Magn Reson Med. 1994; 31(6):673–677. [PubMed: 8057820]

33. Dula AN, Gochberg DF, Valentine HL, Valentine WM, Does MD. Multiexponential T2, magnetization transfer, and quantitative histology in white matter tracts of rat spinal cord. Magn Reson Med. 2010; 63(4):902–909. [PubMed: 20373391]
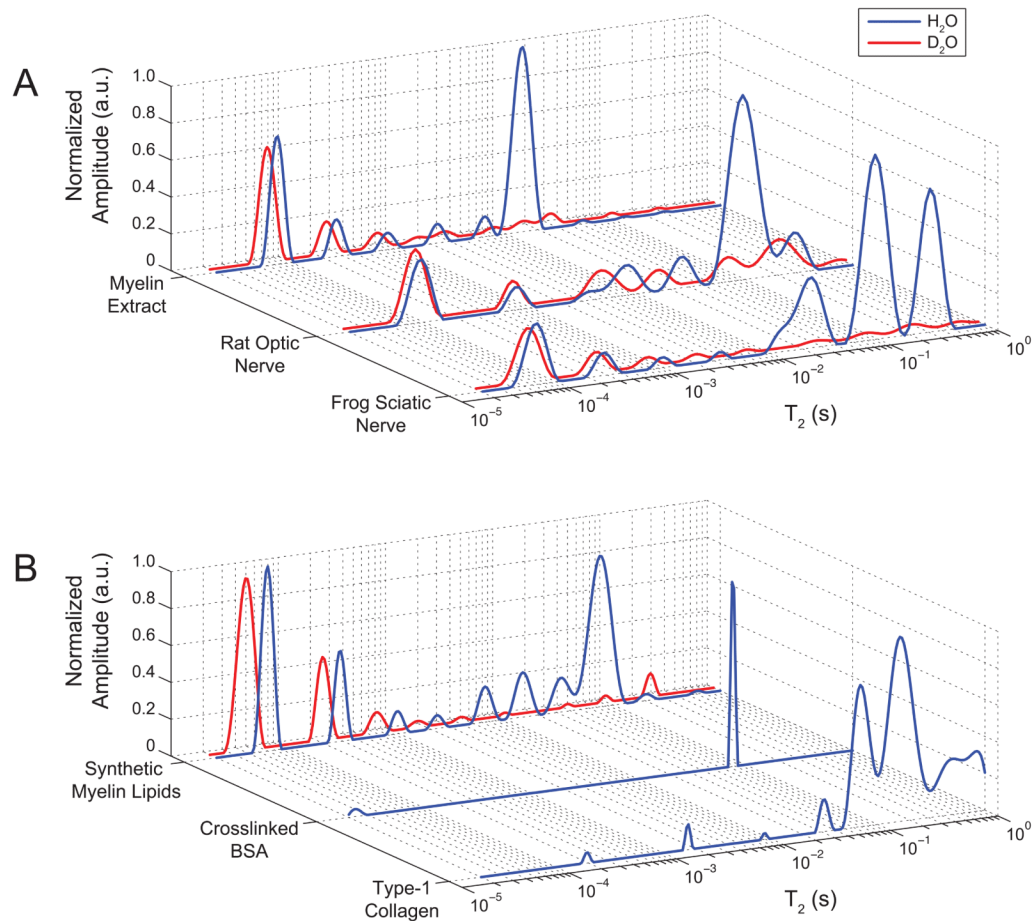
FIGURE 1.
Representative T_2 spectra from biological sources (A) of frog sciatic nerve, rat optic nerve, and bovine brain myelin extract (Phantom I); and T_2 spectra from synthetic sources (B) of refined myelin lipids (Phantom II) and collagen/BSA proteins (Phantoms IIIa/b, respectively), in naturally abundant water (blue/black) or after prolonged D_2O immersion (red/gray). D_2O immersion dilutes ^1H capable of chemical exchange with water, so only methylene ^1H signals effectively survive D_2O immersion. In all sources except the pure protein phantoms (IIIa/b), a large uT_2 component ($\approx$ 60-100 μs) was consistently observed with at least one other longer-lived uT_2 component. All uT_2 components effectively survived D_2O immersion and are attributed predominantly to methylene ^1H. Long-lived T_2s (> 1 ms) are attributed primarily to water ^1H, in agreement with previous studies.
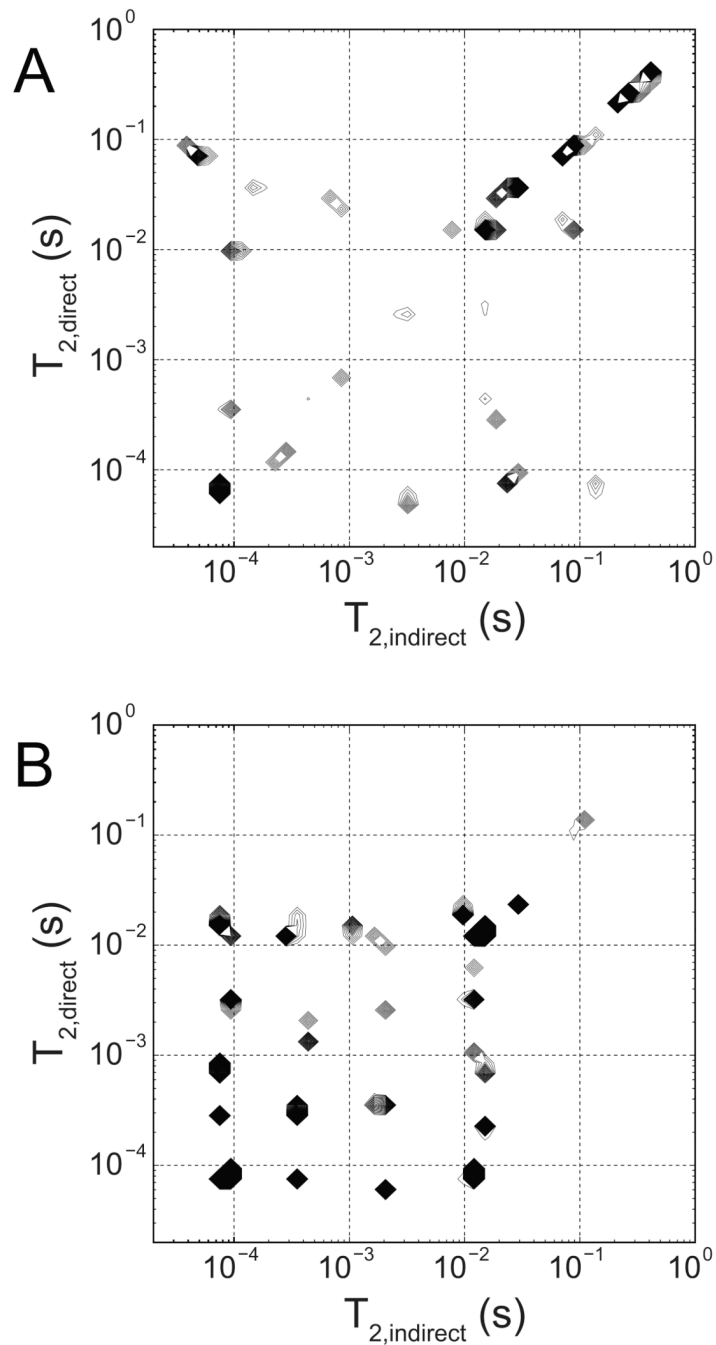
FIGURE 2.
T_2-T_2 exchange spectroscopy (REXSY) spectra from frog sciatic nerve (A) and the bovine brain myelin extract phantom (B). In these contour plots of spectral intensity (higher amplitudes appear darker due to more closely spaced contour lines), components appearing on the main diagonal represent stationary ^{1}H that do not exchange with other sites during the REXSY mixing period. Off-diagonal cross-peaks indicate spins that undergo exchange between corresponding main-diagonal components and are labeled accordingly. Thus, in frog sciatic nerve, ^{1}H exchange occurs among uT_2 components and both the ≈ 25 ms (myelin water) and 90 ms (extra-axonal water) components. Exchange is also observed in the myelin extract phantom between uT_2 components and the main water T_2 (≈ 15 ms),

indicating that myelin/water interactions may give rise to the majority of uT_2-related exchange observed in myelinated frog nerve.
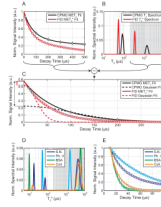
FIGURE 3.
Rapid relaxation in myelin extract (A-C) and in sciatic nerve and phantoms (D,E). (A) CPMG (diamonds) and FID (circles) signal magnitudes from deuterated Phantom I (myelin extract); multi-exponential fits are displayed as solid lines and (B) in the T_2 (or T_2^*) domain. Fitted long-T_2 (or T_2^*) components (gray: $T_2 > 200$ μs) were subtracted from the original data to isolate the (C) shortest-lived signals. Short-lived CPMG data were fitted with exponential (solid black) and Gaussian (dashed black) functions; the exponential fit overestimates the Gaussian signal amplitude by ≈2.5× (black arrow). Short-lived FID data were fitted with exponential (solid red) and Gaussian (dashed red) functions; the exponential fit overestimates the Gaussian signal amplitude by only ≈1.1× (red arrow). *(CPMG and FID signal amplitudes (A&C) are normalized to 1 at t = 0 for display purposes.)* Multi-exponential fits of early FIDs from a sciatic nerve (S.N.), Phantom II (synthetic myelin lipid, Ph. II), BSA protein phantom, and collagen gel phantom (Coll.) are shown in the T_2^* (D) and time (E) domains. As before, fitted long-T_2^* components (D, gray) have been subtracted from FIDs to isolate shortest-lived signals (E). Very short-lived decays ($T_2^* < 20$ μs) were seen in sciatic nerve and the protein phantoms, although such decays were clearly non-exponential. Additionally, a uT_2 component (≈ 70 μs) was observed in sciatic nerve, similar to the myelin phantoms I & II. *(FID amplitudes in (E) are normalized to 1 at the first datum for display purposes.)*
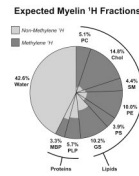
FIGURE 4.
Expected biological myelin ^{1}H fractions, by molecular source. Clockwise, lipid ^{1}H sources are phosphatidylcholine (PC), cholesterol (Chol), sphingomyelin (SM), phosphatidylethanolamine (PE), phosphatidylserine (PS), and gangliosides (GS); protein sources are proteolipid proteins (PLP) and myelin basic protein (MBP); finally, the water source includes surface-bound and interstitial membrane water. Light and dark shading indicate the portions of each molecular source representing non-methylene and methylene ^{1}H, respectively. For example, 5.1% of total myelin ^{1}H is found on phosphatidylcholine, which is predominantly methylene ^{1}H. In bulk myelin, there is a similar amount of expected methylene ^{1}H (all darkly-shaded regions) as compared to myelin water ^{1}H, which is reported in Table 1.

TABLE 1

Observed uT_2 ^1H signal size in myelinated nerves and myelin extract, compared to expected mammalian myelin membrane ^1H content. Total observed uT_2 ^1H and expected ^1H are normalized to the ^1H content of myelin water and are also subdivided into non-methylene (D_2O-exchanging) and methylene portions. Total expected myelin membrane ^1H is further divided into lipid and protein components. It is apparent that observed uT_2 signals are similar in size to the ^1H pools expected in myelin lipids and bulk myelin (see Fig 3). Nerve results are reported as mean ± one standard deviation across all three frogs or as the range for both rats.

	^1H Source	[^1H] / [Myelin water ^1H]		
		Total	*Non-Methylene*	*Methylene*
Observed NMR uT_2 Signals	Frog Sciatic Nerve	1.01 ± 0.07	0.03 ± 0.04	0.98 ± 0.11
	Rat Optic Nerve	1.09 - 1.13	< 0.01	≈ 1.09 – 1.13
	Bovine Brain Myelin Extract	1.12	0.01	1.11
Expected Myelin Membrane ^1H	Myelin Lipids	1.14	0.07	1.07
	Myelin Proteins	0.21	0.07	0.14
	Total Myelin Membrane	1.35	0.14	1.21